Study of Cosmic Ray Interaction Model based on Atmospheric Muons for the Neutrino Flux Calculation

Study of cosmic ray interaction model based on atmospheric muons for the neutrino flux calculation

T. Sanuki[*]

International Center for Elementary Particle Physics, the University of Tokyo, 7-3-1 Hongo, Bunkyo-ku, Tokyo 113-0033, Japan

M. Honda[†] and T. Kajita[‡]

Institute for Cosmic Ray Research, the University of Tokyo, 5-1-5 Kashiwa-no-ha, Kashiwa, Chiba 277-8582, Japan

K. Kasahara[§]

Shibaura Institute of Technology, 307 Fukasaku, Minuma-ku, Saitama 337-8570, Japan

S. Midorikawa[‖]

Faculty of Software and Information Technology, Aomori University, 2-3-1 Kobata, Aomori, Aomori 030-0943, Japan

We have studied the hadronic interaction for the calculation of the atmospheric neutrino flux by summarizing the accurately measured atmospheric muon flux data and comparing with simulations. We find the atmospheric muon and neutrino fluxes respond to errors in the π-production of the hadronic interaction similarly, and compare the atmospheric muon flux calculated using the HKKM04 [M. Honda, T. Kajita, K. Kasahara, and S. Midorikawa, Phys. Rev. D **70,** 043008 (2004).] code with experimental measurements. The $\mu^+ + \mu^-$ data show good agreement in the $1 \sim 30$ GeV/c range, but a large disagreement above 30 GeV/c. The μ^+/μ^- ratio shows sizable differences at lower and higher momenta for opposite directions. As the disagreements are considered to be due to assumptions in the hadronic interaction model, we try to improve it phenomenologically based on the quark parton model. The improved interaction model reproduces the observed muon flux data well. The calculation of the atmospheric neutrino flux will be reported in the following paper [M. Honda *et al.*, Phys. Rev. D **75,** 043006 (2007).].

I. INTRODUCTION

Evidence of neutrino oscillations was found in the atmospheric neutrino data observed with Super-Kamiokande [1]. Atmospheric neutrinos are still a powerful tool to study neutrino oscillations, and the overall uncertainties in the observed data are becoming smaller [2]. It is highly desirable to predict the absolute flux value and ratios among different kind of neutrinos precisely, and to understand their "systematic" uncertainties. Note, atmospheric neutrino experiments cover a wide $L/E(=$ [neutrino flight length]/[neutrino energy]) range, over 4 orders of magnitude [3], which is much wider than accelerator neutrino beam experiments such as K2K [4]. Atmospheric neutrino experiments are complementary to accelerator neutrino experiments, which enable a narrow parameter region to be accurately surveyed.

In order to calculate the atmospheric neutrino intensities precisely, we need detailed information about (i) the primary cosmic-ray spectra at the top of the atmosphere, (ii) the hadronic interactions between cosmic rays and

atmospheric nuclei, (iii) the propagation of cosmic-ray particles inside the atmosphere, and (iv) the decay of the secondary particles.

For (i) the primary cosmic spectra, the uncertainties have been greatly reduced with new measurements of primary cosmic rays [5–8]. Among these experiments, the spectra of cosmic-ray protons reported by AMS and BESS show a very good agreement up to around 100 GeV, although they were carried out in very different experimental conditions. AMS flew on-board the space shuttle orbiting at the altitudes between 320 km and 390 km. On the other hand, BESS was a balloon-borne experiment carried out at the atmospheric depths of about 5 g/cm^2 ($\sim$ 37 km a.s.l.). Then BESS-TeV [9], the upgraded BESS experiment which extended the energy region up to 540 GeV, confirmed the results of AMS and BESS. The results of BESS-TeV agree with that of BESS to within 3%.

We note the observed proton spectrum by CAPRICE is obviously lower than that of AMS or BESS. However, the event number acquired by AMS and BESS is far larger than that of CAPRICE. Although it is difficult to combine the results of the different experiments, a combined analysis using AMS, BESS and CAPRICE data would gives a very close result to that using AMS and BESS only [10]. The difference of Helium spectra observed by AMS and BESS are also sizable. However, as the proton is the dominant component in the cosmic rays, the difference in

---

[*]Electronic address: sanuki@icepp.s.u-tokyo.ac.jp
[†]Electronic address: mhonda@icrr.u-tokyo.ac.jp; http://icrr.u-tokyo.ac.jp/~mhonda
[‡]Electronic address: kajita@icrr.u-tokyo.ac.jp
[§]Electronic address: kasahara@icrc.u-tokyo.ac.jp
[‖]Electronic address: midori@aomori-u.ac.jp

terms of the nucleon flux is less than $\sim 4\%$ below 100 GeV. The nucleon flux is important in the calculation of atmospheric muon and neutrino fluxes. We consider that the cosmic ray is well understood below 100 GeV, which is important for the calculation of atmospheric muons and neutrinos below 10 GeV.

For the study of (ii) the hadronic interactions, the accelerator experiment is the most direct method. However, the data available now do not cover all the phase space necessary for the calculation of atmospheric neutrino flux. We study the hadronic interactions using the atmospheric muon flux data in this paper. As the energy of π or K mostly goes to muons at their decay, the muons are considered to carry essential information of π and K production in the hadronic interactions. There have been a lot of measurements of atmospheric muon flux at ground level as compiled in Ref. [11] and at the balloon altitudes [12–16]. Among them, we select the series of precise measurements of atmospheric muons by BESS at various altitudes; sea level [9], mountain altitude [17] and balloon altitude [18], with sufficiently small systematic and statistical errors. In all these measurements, they used essentially the same apparatus as for the primary cosmic-ray measurements [7,9], and systematic errors were well controlled. There are other precision measurements of the atmospheric muon flux useful for the study in this paper, such as the L3 + C experiment [19].

Our study might be compared with the direct calculation of atmospheric neutrino flux from the atmospheric muon flux [20–22], in which the π's are assumed as the dominant source of the atmospheric neutrinos and muons. The calculation was reviewed in Ref. [23]. The differences of our study from those works are in the use of a well-constructed model of primary cosmic-ray spectra, and a full Monte Carlo simulation code for atmospheric muon and neutrino fluxes calculation. Then we study the hadronic interactions comparing the calculated and observed atmospheric muon fluxes. Both the model of primary cosmic-ray spectra and the simulation code are the same as those used in HKKM04 calculation [24]. The primary flux model is very close to that constructed in Refs. [10,25] based on the AMS and BESS data. We use the primary flux model with a modification of the spectrum index of cosmic-ray protons from -2.74 to -2.71 above 100 GeV, according to the emulsion chamber experiments at higher energies [26,27]. The simulation code treat the (iii) propagation of cosmic-ray particles inside the atmosphere and (iv) decay of the secondary particles sufficiently accurately.

Calculating the atmospheric neutrino flux from the primary cosmic-ray flux, the atmospheric muon flux was also used to calibrate the calculation in Ref. [28]. However, the atmospheric density profile is crucial in this study.

First, we review the precision measurements of muon flux by BESS and other instruments in Sec. II. Next, we study what kind of information can be deduced from the comparison of the calculation of atmospheric muon flux and observed data for the calculation of atmospheric neutrino flux in Sec. III. We also study the effect of the atmospheric density profile on the muon flux in Sec. IV before the comparison. Note, the seasonal change of the air density profile causes $\pm 5\%$ variations of muon flux at ~ 1 GeV/c at sea level. And even larger variation is expected to result from changes in local meteorological conditions. In the same section we also discuss the effect of the uncertainty of the interaction cross section between cosmic rays and air nuclei.

We calculate the muon fluxes in the HKKM04 scheme with the observed atmospheric density profile, and compared them with the precisely measured muon flux data, in Sec. V. Note, the existence of precise atmospheric density profile data during the observation period is another important reason that we use the muon flux data from the BESS measurements. We find $\mu^+ + \mu^-$ shows reasonable agreement in the $1 \sim 30$ GeV/c range between the calculations and observations, but that the agreement worsens above 30 GeV/c. In addition, the μ^+/μ^- ratio shows a sizable difference. The difference is considered to be due to errors in the hadronic interaction model used in HKKM04 (DPMJET-III [29]).

We try to improve the hadronic interaction model in Sec. VI, and compared with the data from recent accelerator data [30]. With a phenomenological consideration based on quark parton model, K productions are also modified in this "improvement." As the result of the modification, the observed muon fluxes are reproduced with good accuracy (Sec. VII).

Note, the available precision muon flux data are essentially those for the vertical directions. If we have the accurately measured horizontal muon flux data, we can test the simulation code by the comparison of the calculated and observed muon fluxes for the horizontal directions. This comparison would be a good support for our procedure. However, the muon flux data for horizontal direction are poorer than those for vertical directions. We just show the comparison of the calculation and available muon flux data for horizontal directions [31,32] in Sec. VII. The calculation of atmospheric neutrino flux with the modified interaction model will be reported in the following paper [33].

II. PRECISION MEASUREMENTS OF ATMOSPHERIC MUON

The BESS group performed a series of atmospheric muon observations at various levels and sites; balloon altitude, mountain altitude and at sea level.

At balloon altitudes, where the atmospheric depths ($5 \sim 25$ g/cm^2) are much smaller than the interaction mean free path of protons (~ 100 g/cm^2), the muon flux measurement is considered as an inclusive experiment with the

primary cosmic-ray beam and the air nucleon target. We can expect rich information about hadronic interactions from this region. However, only a small number of experiments had been performed, and their data are poor in statistics, because the muon flux itself is small at balloon altitudes and the observation time is limited. On January 24th, 2001, the BESS group carried out a muon flux observation at balloon altitudes with exceptionally good statistics at Fort Sumner, NM, USA [18]. After reaching an altitude with a residual atmospheric depth of 5 g/cm^2, the balloon slowly descended to 28 g/cm^2 in 12.4 h. A large number of primary and secondary cosmic rays were recorded during the descending period. The positive muon spectrum was obtained for 0.50–2.55 GeV/c and negative muon spectra for 0.50–9.76 GeV/c. As discussed in Ref. [34], we selected DPMJET-III as the interaction model for HKKM04 with these muon data, since it reproduced the observed atmospheric muon spectra better than the interaction models of Fritiof 1.6 [35], Fritiof 7.02 [36], and FLUKA'97 [37].

The BESS group has also measured the atmospheric muon flux for vertical directions at ground level; at Mt. Norikura, Japan (742 g/cm^2) in September, 1999 [17] and at Tsukuba, Japan (1032 g/cm^2) in October, 2002 [9]. The momentum ranges covered are 0.58–106 GeV/c at Norikura and 0.58–404 GeV/c at Tsukuba. In both experiments, the observation times were long enough that the systematic errors dominate the statistical errors. The overall errors were 3% at 1 GeV/c, 3% at 10 GeV/c, and 9% at 100 GeV/c for the Norikura experiment, 2% at 1 GeV/c, 3% at 10 GeV/c, and 5% at 100 GeV/c for the Tsukuba experiment. Note that the Tsukuba experiment was carried out with the BESS-TeV detector, which could not distinguish electrons and positrons from muons [9]. On the other hand, the BESS detector used for the Norikura experiment was equipped with an electromagnetic shower counter to distinguish electrons and positrons from muons [17]. As an important aspect of the muon measurement by BESS at ground level, the precise atmospheric density profile data are available from the Japan Meteorological Agency [38].

The L3 + C detector has measured the atmospheric muon flux accurately from 20 GeV/c to 3 TeV/c and at zenith angles from 0° to 58° at CERN [19]. The L3 + C detector was originally constructed for the LEP experiment as the L3 muon spectrometer, and the efficiency and the absolute momentum scale were calibrated with the muon pairs from Z decays. The overall error is read from Ref. [19] to be 4.5% at 20 GeV/c, less than 3% in 60–500 GeV/c, and 10% at 1.5 TeV/c. However, the L3 + C detector is situated below a molasses overburden of 30 m (6854 g/cm^2), which could be a source of unknown systematic error at lower momenta. In the following study, we used the L3 + C data for vertical directions ($\cos\theta_{\text{zenith}} > 0.9$), and in the momentum range of 60 GeV/c–3 TeV/c.

For the horizontal directions, there are muon flux data from the MUTRON [32] and DEIS [31] experiments at sea level. MUTRON observed the muon flux from 100 GeV/c to 20 TeV/c in momentum and from 86° to 90° (88.9° on average) in zenith angle, and DEIS from 10 GeV/c to 10 TeV/c in momentum and from 78° to 90° in zenith angle. However, it is difficult to read the systematic errors from their reports [31,32]. These data are potentially useful to study the validity of the simulation code at higher energies, rather than to study the hadronic interaction model.

III. RESPONSE OF ATMOSPHERIC MUON AND NEUTRINO FLUXES TO ERRORS IN HADRONIC INTERACTIONS

Before a study of the hadronic interactions, we look at the response of atmospheric muon and neutrino fluxes to errors in the hadronic interaction model. If their responses are the same, we can study the hadronic interactions relevant to the atmospheric neutrino flux with the atmospheric muon flux data. Here, we derive some analytical expressions for the calculation of atmospheric muon and neutrino fluxes, but we actually calculate them in the Monte Carlo simulation, then interpret the results with the analytical expressions.

We use the HKKM04 calculation code for the Monte Carlo calculation of atmospheric neutrino flux [24]. In the HKKM04 scheme, the primary cosmic-ray flux model based on the AMS and BESS observations [10,25] was used with a modification of the spectrum index for proton cosmic rays from -2.74 to -2.71 above 100 GeV, so that the extension goes through the center of the emulsion experiment data [26,27] at higher energies. DPMJET-III [34] was selected for the hadronic interaction model, and the US-Standard '76 [39] atmospheric density profile was used. Note, however, the discussion in this section is not sensitive to the details of the Monte Carlo simulation scheme.

To cut out the hadronic interactions, we write the atmospheric lepton (μ, ν_μ, or ν_e) fluxes as

$$\phi_l(p_l) = \sum_{m=\pi^\pm, K^\pm, K^0_L, K^0_S} \int_h T^l_m(p_m, p_l, h) \cdot Y^m(p_m, h) dp_m dh, \qquad (1)$$

where l stands for the kind of lepton, m stands for the kind of meson ($\pi^\pm$, $K^\pm$, . . .), $T^l_m(p_m, p_l, h)$ is the probability with which the m-meson produced with momentum p_m and at altitude h creates an l-lepton with momentum p_l at ground level, and $Y^m(p_m, h)$ is the m-meson yield spectrum at the altitude h. As the mesons are created in the hadronic interaction of cosmic rays and air nuclei, the $Y^m(p_m, h)$ is written as

$$Y^m(p_m, h) = \int_{p_{\text{proj}}} \rho_{\text{air}}(h) \cdot \sum_i \sigma_i(p_{\text{proj}}) \cdot \eta_i^m(p_{\text{proj}}, p_m)$$
$$\cdot \phi_i(p_{\text{proj}}, h) dp_{\text{proj}}, \tag{2}$$

where $\rho_{\text{air}}(h)$ is the nuclear density of the air at altitude h, i stands for the kind of projectile $(p, \bar{p}, \ldots, \pi^{\pm}, \ldots)$ for the hadronic interaction in the atmosphere, σ_i is the hadronic production cross section of the i particle and the air nuclei, $\eta_i^m(p_{\text{proj}}, p_m)$ is the m-meson production spectrum in the hadronic interaction of i projectile and air nuclei, and $\phi_i(p_{\text{proj}}, h)$ is the momentum spectrum of i particle at altitude h. Note, we assume the superposition model for cosmic rays heavier than protons.

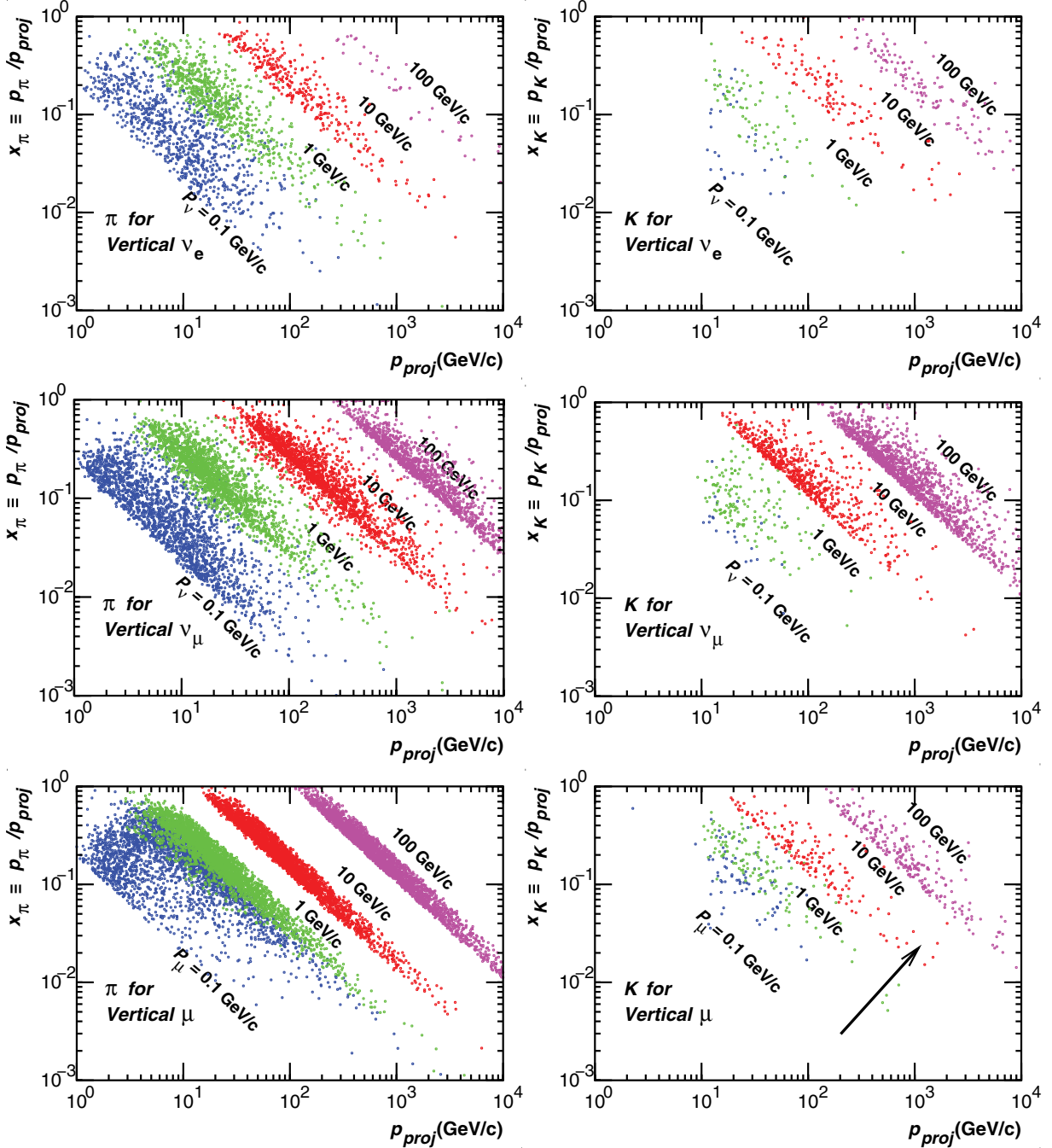Substituting Eq. (2) in Eq. (1) and changing the integration order, we obtain

FIG. 1 (color online). The scatter plot of π's (π^+ and π^-, left) and K's ($K^{\pm}$, K_L^0, and K_s^0, right) in the phase space (p_{proj}-x plane) at their production relevant to atmospheric μ's and ν's at the momenta, 0.1, 1.0, 10, and 100 GeV/c, at sea level for vertical directions. Here, x is defined as $x \equiv p_m/p_{\text{proj}}$ in the rest frame of Air nuclei for $m = \pi$ or K. We sampled 3000 μ's and 3000 ν's ($\nu_e + \nu_{\mu}$) at each momentum from the HKKM04 calculation. The arrow in the right bottom panel shows the directions to which $p_{\pi,K}$ increase.

$$\phi_l(p_l) = \sum_m \int_{p_m} \int_{p_{proj}} \left[\int_h T_m^l(p_m, p_l, h)\rho_{air}(h) \right.$$

$$\times \sum_i \sigma_i(p_{proj})\eta_i^m(p_{proj}, p_m)\phi_i(p_{proj}, h)dh \Big]$$

$$\times dp_{proj}dp_m, \tag{3}$$

The term inside the square brackets in Eq. (3) is interpreted as the contribution density in meson production phase spaces (p_{proj}-p_m plane) to the lepton flux. Using the scaling variable $x \equiv p_m/p_{proj}$ defined in the rest frame of Air nuclei, we show the contribution density calculated by the Monte Carlo calculation as a scatter plot in p_{proj}-x plane (Fig. 1). Note, the variable x is defined in the rest frame of Air nuclei.

Here, we sampled 3000 μ's ($\mu^+ + \mu^-$) and 3000 ν's ($\nu_\mu + \bar{\nu}_\mu + \nu_e + \bar{\nu}_e$) at 0.1, 1.0, 10, and 100 GeV/c from the HKKM04 calculation for atmospheric μ and ν fluxes for vertical directions at sea level. Then, we plotted the momenta of parent mesons, π's (π^+ and π^-) or K's ($K^\pm$, K_L^0 and K_s^0), and projectiles in Fig. 1 as a scatter plot. Note, here and in the following discussions in this section, we do not distinguish the particles from antiparticles.

For the μ's, ν_μ's, and ν_e's, most π's or K's are concentrated in narrow stripes for each momentum above 1 GeV/c. In Fig. 2. we project the points to the π or K momentum axis (left) and to the x axis (right) and show them in histograms. The total number of μ's or ν's ($\nu_e + \nu_\mu$) is normalized to 3000 for each momentum as in the scatter plot (Fig. 1). However, the histograms for the ν_e at 100 GeV/c are multiplied by a factor of 5, due to the rapid decrease of ν_e at this momentum. The projections to the meson momentum axis are narrow distributions with sharp peaks both for π's and K's, which is proportional to the integrand of the p_m integration in Eq. (3). The projections to x axis are very much like each other for all the μ's, ν_μ's, and ν_e's above 1 GeV/c. The projections to x axis at 10 GeV/c are not shown in the figure, since they are almost the same to those at 1 GeV/c or 100 GeV/c.

Changing the integration variables from $dp_{proj}dp_m$ to $(p_m/x^2)dxdp_m$, and exchanging the integration order, Eq. (3) can be rewritten as

$$\phi_l(p_l) = \sum_m \int_x \left[\int_{p_m} \int_h T_m^l(p_m, p_l, h)\rho_{air}(h) \sum_i \left\{ \sigma_i\left(\frac{p_m}{x}\right) \right. \right.$$

$$\left. \left. \cdot \eta_i^m\left(\frac{p_m}{x}, p_m\right) \cdot \phi_i\left(\frac{p_m}{x}, h\right) \right\} dh \frac{p_m}{x^2} dp_m \right] dx. \tag{4}$$

The projection to the x axis is proportional to the integrand of the x integration, and it is directly connected to the hadronic interaction model. To illustrate this we introduce some assumptions. First, we assume all the projectiles are nucleons. In Fig. 3, we plot the relative composition of the projectiles for the interactions in which the parent meson of the leptons are created in the HKKM04 calculation. We find the major projectiles are nucleons below 100 GeV/c, and the contribution of meson projectile remains $\lesssim 15\%$ even at higher momenta.
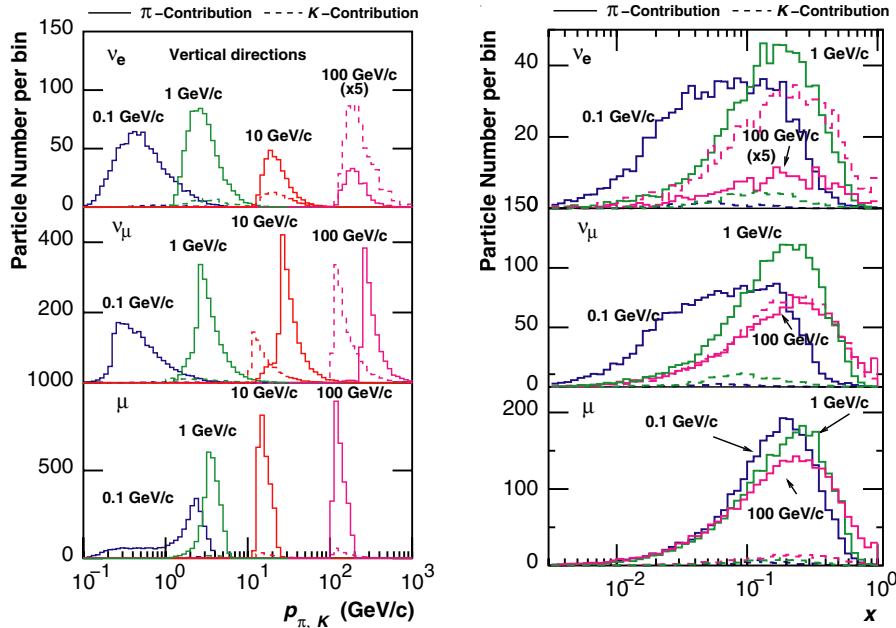

FIG. 2 (color online). Left panel: the momentum distributions of π's and K's relevant to the atmospheric μ's and ν's with fixed momenta, 0.1, 1.0, 10, 100 GeV/c, at sea level for vertical directions. Right panel: the corresponding x distributions for all except $p_{\mu,\nu} = 10$ GeV/c. In these figures, total number of μ's or ν's ($\nu_e + \nu_\mu$) is normalized to 3 000 but the histograms are multiplied by a factor of 5 for ν_e at 100 GeV/c.
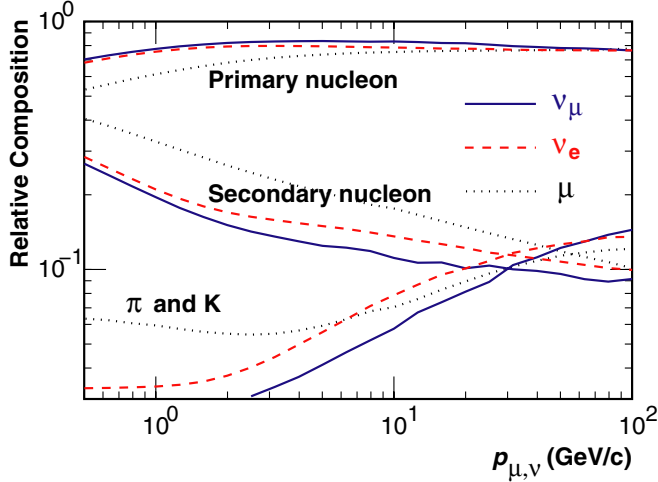
FIG. 3 (color online). The relative composition of the projectile of the last hadronic interaction, for atmospheric μ, ν_μ, and ν_e.

Next, as the width of the p_m distributions for fixed p_l is narrow in the left panel of Fig. 2, we approximate it with the δ function (zero width approximation) and write $T_m^l(p_m, p_l, h)$ as

$$T_m(p_m, p_l, h) = \bar{T}_m^l(p_m, h) \cdot \delta(p_m - P_{ml}(p_l, h)), \quad (5)$$

where $p_m = P_{ml}(p_l, h)$ is the average relation between p_m, the momentum of mesons at altitude h, and p_l, the momentum of leptons at ground. Then the p_m integration is easily carried out and Eq. (4) is rewritten as

$$\phi_l(p_l) = \sum_m \int_x \int_h \bar{T}_m^l(p_m, h) \rho_{\text{air}}(h) \sigma_N\left(\frac{p_m}{x}\right) \cdot \phi_N\left(\frac{p_m}{x}, h\right)$$
$$\cdot \eta_N^m\left(\frac{p_m}{x}, p_m\right) dh \frac{p_m}{x^2} \, dx, \qquad (6)$$

with $p_m = P_{ml}(p_l, h)$. Note, as we are working with the flux sum of particles and antiparticles in this section, we introduced the isosymmetric m production function:

$$\eta_N^m(p_{\text{proj}}, p_m) \equiv (\eta_p^m(p_{\text{proj}}, p_m) + \eta_n^m(p_{\text{proj}}, p_m))/2, \quad (7)$$

for nucleons. Note, the argument h in the P_{ml} is introduced to account for the energy loss of μ for the leptons which are produced by μ decay. The energy loss of the mesons before decay is very small. The variation of the production height is estimated as $\sim \pm 100$ g/cm^2, since the mean free path of the cosmic rays is 100 g/cm^2. Therefore, the variation of p_m due to the variation of production height is $\sim \pm 0.2$ GeV/c from the average, which is sufficiently small for leptons above 1 GeV/c. We can write the relation of p_m and p_l in a much simpler function as $p_m = P_{ml}(p_l)$ without any altitude dependence for $p_l \gtrsim 1$ GeV/c. Then $\eta_N^m(p_m/x, p_m)$ comes out of the h integration in Eq. (6), and it is rewritten as

$$\phi_l(p_l) = \sum_m \int_x \left[\int_h \bar{T}_m^l(p_m, h) \rho_{\text{air}}(h) \sigma_N\left(\frac{p_m}{x}\right) \right.$$
$$\left. \cdot \phi_N\left(\frac{p_m}{x}, h\right) dh \right] \cdot \left[\eta_N^m\left(\frac{p_m}{x}, p_m\right) \frac{p_m}{x^2} \right] dx, \quad (8)$$

for $p_l \gtrsim 1$ GeV/c. Now, the projection of contribution density to the x axis is expressed by the product of two terms. One stands for the hadronic interactions, and the other for the rest. For later convenience, we write the expression as

$$\phi_l(p_l) = \sum_m \phi_{l(m)}(p_l) = \sum_m \int_x H_m^l(p_m, x) dx, \quad (9)$$

with $p_m = P_{ml}(p_l)$ for $l = \mu$, ν_μ, ν_e, and $m = \pi^\pm, K^\pm, \cdots$. We will come back to the validity of the zero width approximation later.

Here, we note it is difficult to study the hadronic interactions for K productions with atmospheric μ fluxes. In Fig. 4, we depicted the contribution of K's to the atmospheric μ's and ν's in the ratio to the total flux as the functions of momentum. The K-contribution is limited to the atmospheric μ's below 1 TeV/c, while that the K-contribution to atmospheric ν is sizable above 10 GeV/c, and is dominant above 100 GeV/c for vertical directions. However, as most atmospheric μ's are produced in the π-decays, we can use them to study the π productions in the hadronic interactions, which are important in the calculation of atmospheric ν flux below 100 GeV/c.

We continue the study of hadronic interactions concentrating on the π productions. In the following, we compare the variations of the different lepton fluxes due to the error in the π production of the hadronic interaction model. This comparison should be done at the momentum where the parent π's momenta are the same. Therefore, the momentum relation $p_\pi = P_{\pi l}(p_l)$ is necessary for this study. We construct the function from the Monte Carlo data, averaging the parent π's momenta for a fixed lepton momentum. However, the comparison is carried out among the fluxes of different kinds of leptons. Therefore, we show the momentum relation between μ's and ν_μ's, μ's, and ν_e's as ratios, namely $P_{\pi\mu}^{-1}(P_{\pi\nu_\mu}(p_{\nu_\mu}))/p_{\nu_\mu}$ and $P_{\pi\mu}^{-1}(P_{\pi\nu_e}(p_{\nu_e}))/p_{\nu_e}$, in Fig. 5. The ratio for horizontal directions is taken between horizontal ν_μ or ν_e and vertical μ. Note, the average momentum of parent π for μ's are limited to $\gtrsim$ 2 GeV/c, since it is difficult for μ's produced in the decay of π's with lower momenta than this limit to reach the ground level (see Fig. 2). Therefore, there are no corresponding p_μ for p_{ν_μ} or $p_{\nu_e} \lesssim 0.5$ GeV/c. Note, the relation depends on π's energy spectrum at decay, therefore, on the primary cosmic-ray spectra and interaction model. However, changes in these do not affect the relations greatly.
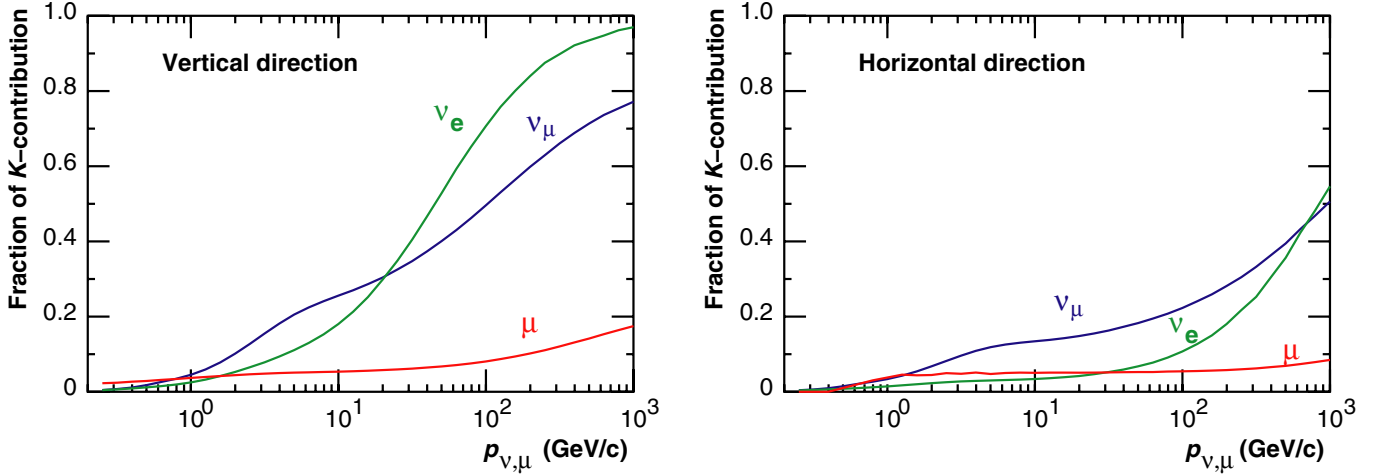
FIG. 4 (color online).   The K-contribution to the vertical μ's and ν's (left), and to the horizontal μ's and ν's (right).

Let us consider that there are 2 interaction models with the hadronic π production function $\eta_N^\pi(p_\pi/x, p_\pi)$ and $\eta_N'^\pi(p_\pi/x, p_\pi)$, and assume they are related by the factor function $\zeta(p_\pi/x, x)$ as

$$\eta_N'^\pi\left(\frac{p_\pi}{x}, p_\pi\right) = \zeta\left(\frac{p_\pi}{x}, x\right) \cdot \eta_N^\pi\left(\frac{p_\pi}{x}, p_\pi\right). \quad (10)$$

We will call $\eta_N'^\pi(p_\pi/x, p_\pi)$ the ζ-modification of $\eta_N^\pi(p_\pi/x, p_\pi)$. The ζ-modified lepton fluxes are calculated as

$$[\phi_{l(\pi)}(p_l)]_\zeta = \int_x \zeta\left(\frac{p_\pi}{x}, x\right) \cdot H_\pi^l(p_\pi, x)dx, \quad (11)$$

where $p_\pi = P_{\pi l}(p_l)$ for $l = \mu$, ν_μ, and ν_e. Note, the error of the π production function is also considered as a modi-
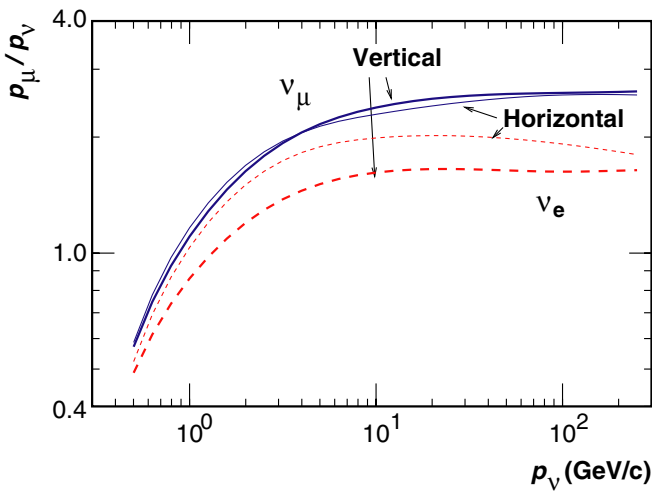

FIG. 5 (color online).   The momentum ratio of μ's to ν_μ's or ν_e's, whose parent π momenta are the same on average. The "Horizontal" in the figure means the momentum ratio between vertical μ's and horizontal ν_μ's or ν_e's.

fication of the π production function of the perfect interaction model.

Using Eq. (11) and the results of the Monte Carlo calculation partly shown in Fig. 2, it is now easy to study the effect of an error in the π production function on the fluxes of μ, ν_μ, and ν_e, with test functions for ζ. We assume that the modification function is expanded in the 2nd order B-spline functions [40] as

$$\zeta\left(\frac{p_\pi}{x}, x\right) = 1 + \sum_i C_{\zeta,i}\left(\frac{p_\pi}{x}\right) \cdot \xi_i(\log(x)), \quad (12)$$

where the 2nd order b-spline functions use here are defined as

$$\xi_i(u) = \frac{1}{2} \times \begin{cases} \left(\frac{u-u_i}{\Delta}+1.5\right)^2 & \left(-1.5 \le \frac{u-u_i}{\Delta} < -0.5\right) \\ 1.5 - 2\left(\frac{u-u_i}{\Delta}\right)^2 & \left(-0.5 \le \frac{u-u_i}{\Delta} < 0.5\right) \\ \left(\frac{u-u_i}{\Delta}-1.5\right)^2 & \left(0.5 \le \frac{u-u_i}{\Delta} < 1.5\right) \end{cases}$$

and $\xi_i(u) = 0.$ $\left(\frac{u-u_i}{\Delta} < -1.5, \text{or} 1.5 \le \frac{u-u_i}{\Delta}\right), \quad (13)$

with $u_i = u_0 + i \cdot \Delta_u$ for $u = \log(x)$. The B-spline function is often used to approximate a general continuous function. It has a compact value region and is normalized as $\sum_i \xi_i(u) = 1$. The differentiability is not important here. Note, when a function is approximated with the expansion of the B-spline functions, the variations quicker than Δ are suppressed.

Then, Eq. (11) can be rewritten as

$$[\phi_{l(\pi)}(p_l)]_\zeta = \int_x \left[1 + \sum_i C_{\zeta,i}\left(\frac{p_\pi}{x}\right)\xi_i(\log(x))\right]$$
$$\cdot H_\pi^l(p_\pi, x)dx, \quad (14)$$

and the difference to the original flux as

$$[\delta\phi_{l(\pi)}(p_l)]_\zeta \equiv [\phi_{l(\pi)}(p_l)]_\zeta - \phi_{l(\pi)}(p_l)$$

$$= \sum_i C_{\zeta,i}\left(\frac{p_\pi}{x}\right) \cdot \int_x \xi_i(\log(x))$$

$$\cdot H_\pi^l(p_\pi, x)dx. \tag{15}$$

Therefore, the relative difference is calculated as

$$\frac{[\delta\phi_{l(\pi)}(p_l)]_\zeta}{\phi_{l(\pi)}(p_l)} = \frac{\sum_i C_{\zeta,i}(p_\pi/x)\int_x \xi_i(\log(x)) \cdot H_\pi^l(p_\pi, x)dx}{\int_x H_\pi^l(p_\pi, x)dx}$$

$$= \sum_i C_{\zeta,i}\left(\frac{p_\pi}{x}\right) \cdot R_i^l(p_\pi) \tag{16}$$

where

$$R_i^l(p_\pi) = \int_x \xi_i(\log(x)) \cdot H_\pi^l(p_\pi, x)dx \Big/ \int_x H_\pi^l(p_\pi, x)dx, \tag{17}$$

and $p_\pi = P_{\pi l}(p_l)$ for $l = \mu$, ν_μ, and ν_e.

The modification function corresponding to the error from the perfect π production function is expected to be a slowly varying function of x and not very different from 1 in all x regions. In the comparison of the π production between an interaction model and the accelerator experiment data, we find typically differences of $20 \sim 30\%$ (see, for example, Fig. 15 of Ref. [25]).

Applying the Monte Carlo data to H_π^l in Eq. (17), we can consider the artificial modifications of the π productions function with random numbers for 100% error in π production function. Taking a set of uniform random numbers in $[-1, 1]$ for each $\{C_{\zeta,i}\}$, we calculate the variation of $[\delta\phi_\mu]_\zeta/\phi_\mu$, $[\delta\phi_{\nu_\mu}]_\zeta/\phi_{\nu_\mu}$ and $[\delta\phi_{\nu_e}]_\zeta/\phi_{\nu_e}$, using the Eq. (16) and $\Delta = 0.5$ in Eq. (13). The variations for 3000 random $\{C_{\zeta,i}\}$ sets are plotted as a scatter plot in Fig. 6. Although the variations for the $[\delta\phi_\mu]_\zeta/\phi_\mu$, $[\delta\phi_{\nu_\mu}]_\zeta/\phi_{\nu_\mu}$ or $[\delta\phi_{\nu_e}]_\zeta/\phi_{\nu_e}$ are large, we find a narrow

concentrations to the $[\delta\phi_\mu]_\zeta/\phi_\mu = [\delta\phi_\nu]_\zeta/\phi_\nu$ line there.

As $C_{\zeta,i}$ varies freely in $[-1, 1]$, the maximum difference is calculated as

$$\max \left| \frac{[\delta\phi_{\nu(\pi)}(p_\nu)]_\zeta}{\phi_{\nu(\pi)}(p_\nu)} - \frac{[\delta\phi_{\mu(\pi)}(p_\mu)]_\zeta}{\phi_{\mu(\pi)}(p_\mu)} \right|$$

$$= \max \left| \sum_i C_{\zeta,i}[R_i^\nu(p_\pi) - R_i^\mu(p_\pi)] \right|$$

$$= \sum_i |R_i^\nu(p_\pi) - R_i^\mu(p_\pi)|, \tag{18}$$

where ν stands for ν_μ and ν_e. In Fig. 7, we show the maximum difference between $[\delta\phi_\mu]_\zeta/\phi_\mu$ and $[\delta\phi_{\nu_\mu}]_\zeta/\phi_{\nu_\mu}$, and $[\delta\phi_\mu]_\zeta/\phi_\mu$ and $[\delta\phi_{\nu_e}]_\zeta/\phi_{\nu_e}$ as a function of p_ν, and they are small for $p_\nu \gtrsim 1$ GeV/c. Note, for the horizontal directions, the maximum difference between horizontal ν's and vertical μ is calculated. If we assume 20% as the maximum error for the π production function, $C_{\zeta,i}$ is sampled in $[-0.2, 0.2]$ instead of $[-1, 1]$. Then, the maximum differences are multiplied by 0.2 to the values shown in Fig. 7.

For the modifications, or for the error of the hadronic π production function, we have the approximate relation

$$\frac{[\delta\phi_\mu(p_\mu)]_\zeta}{\phi_\mu(p_\mu)} \simeq \frac{[\delta\phi_{\nu_\mu}(p_{\nu_\mu})]_\zeta}{\phi_{\nu_\mu}(p_{\nu_\mu})} \simeq \frac{[\delta\phi_{\nu_e}(p_{\nu_e})]_\zeta}{\phi_{\nu_e}(p_{\nu_e})}, \tag{19}$$

for the lepton flux whose parent momenta are the same, or $P_{\pi\mu}(p_\mu) = P_{\pi\nu_\mu}(p_{\nu_\mu}) = P_{\pi\nu_e}(p_{\nu_e})$. Note, the approximate relation becomes invalid below ~ 1 GeV/c, as is seen from Fig. 7.

The maximum difference with $\Delta = 0.25$ for the B-spline functions [Eq. (13)] is shown with a dashed line in Fig. 7. However, the maximum difference with $\Delta = 0.25$ is almost the same as that with $\Delta = 0.5$, implying $\Delta = 0.5$ is fine enough in this study.
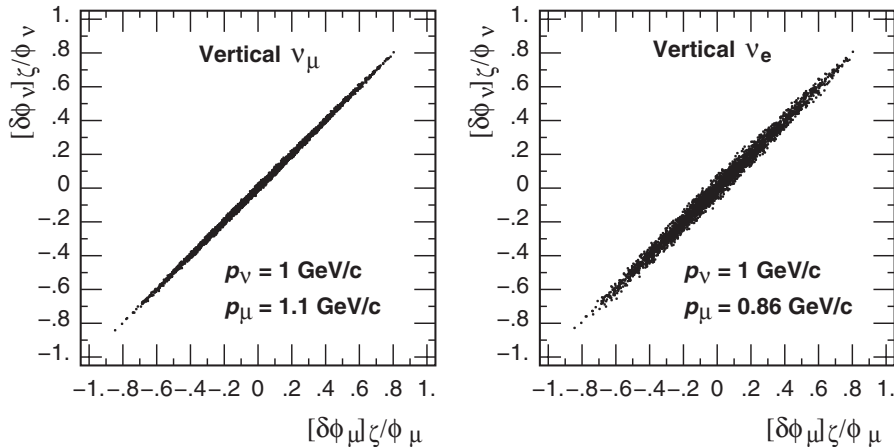

FIG. 6. The scatter plots of $([\delta\phi_\mu]_\zeta/\phi_\mu, [\delta\phi_\nu]_\zeta/\phi_\nu)$ for ν_μ (left) and ν_e (right). The variation is calculated for 3000 sets of random $\{C_{\xi i}\}$ in $[-1, 1]$ for vertical directions at $p_\nu = 1$ GeV/c.
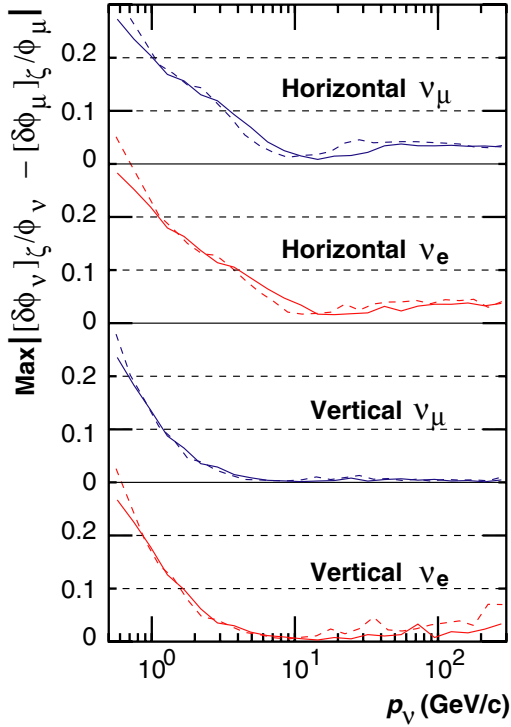
FIG. 7 (color online). The maximum of $|[\delta\phi_{\nu_\mu}]_\zeta/\phi_{\nu_\mu} - [\delta\phi_\mu]_\zeta/\phi_\mu|$ and $|[\delta\phi_{\nu_e}]_\zeta/\phi_{\nu_e} - [\delta\phi_\mu]_\zeta/\phi_\mu|$. The solid line assumes $\Delta = 0.5$ for the B-spline functions [Eq. (13)], and the dashed line $\Delta = 0.25$. They are calculated analytically using the Monte Carlo data.

We have some comments for the zero width approximation. This approximation is valid for the μ's until the variation of the μ-energy lost in the air becomes crucial. This is because the energy of μ in π-decay is limited to

$$\left(1 - \beta \cdot \frac{m_\pi^2 - m_\mu^2}{m_\pi^2 + m_\mu^2}\right) \cdot \bar{E}_\mu \leq E_\mu$$

$$\leq \left(1 - \beta \cdot \frac{m_\pi^2 - m_\mu^2}{m_\pi^2 + m_\mu^2}\right) \cdot \bar{E}_\mu,$$

(20)

or approximately in $0.73 \cdot \bar{E}_\mu \leq E_\mu \leq 1.27 \cdot \bar{E}_\mu$, where $\bar{E}_\mu = E_\pi \cdot (m_\pi^2 + m_\mu^2)/2m_\pi$ is the average energy of μ in π-decay. However, the E_{ν_μ} in the π-decay distributes uniformly in $[0, 2\bar{E}_{\nu_\mu}]$, where $\bar{E}_{\nu_\mu} = E_\pi \cdot (m_\pi^2 - m_\mu^2)/2m_\pi$ is the average energy of E_{ν_μ} in the π decay. For the decay products of the μ's, the 3-body decay phase space is convoluted. Therefore, a wide momentum distribution is expected for the momenta of parent π's of ν's. Note, the μ spin effect is a minor effect in this discussion. However, the steep π-decay spectrum makes the momentum distributions effectively narrower. Most of the momenta of parent π's distribute within $\bar{p}_\pi/2 \lesssim p_\pi \lesssim 2\bar{p}_\pi$, where $\bar{p}_\pi$ is the average momentum of parent π's. Modifying the delta-function in Eq. (5) to a narrow distri-

bution function of p_m and retaining p_m integration in the Eq. (9), we could carry out a more general study than that presented here. However, we expect an almost the same result due the weak dependence of the $\eta_N^m(p_{\mathrm{proj}}, p_m)$ on p_{proj}.

In this section, we have studied the response of atmospheric μ and ν fluxes to error in the π production in the hadronic interaction model. We have shown that a modification affects the atmospheric μ and ν fluxes originating from the π decay at the same rate, namely $\Delta\phi_\mu/\phi_\mu \simeq \Delta\phi_{\nu_\mu}/\phi_{\nu_\mu} \simeq \Delta\phi_{\nu_e}/\phi_{\nu_e}$, for $p_\nu \gtrsim 1$ GeV/c. This is an important relation, since the error of the hadronic interaction model could be sensed by a comparison of calculated and observed μ flux data, especially when accurately measured μ flux data are available. The relation could be used not only to estimate the error in the calculation but also to tune the hadronic interaction model. However, this is true only when we carry out the height integration in Eq. (8) for μ and ν correctly. In other words, the propagation of particles in the air must be carried out correctly (disregarding the hadronic interactions). For an error of the physical input which works in the same direction for the atmospheric μ and ν fluxes, like an error in the primary cosmic-ray flux model, the uncertainty may be merged in the uncertainty of the hadronic interaction model, and is calibrated by the atmospheric muon flux data collectively. However, there are some physical inputs whose error works in different directions for the atmospheric μ and ν fluxes. We must be careful about such uncertainties.

IV. ATMOSPHERIC DENSITY PROFILE AND INTERACTION CROSS SECTION

In this section, we study the effects of error in the atmospheric density profile and hadronic interaction cross section on the atmospheric muon and neutrino fluxes. Both effects are relatively smaller than those of hadronic interaction and primary cosmic-ray flux, but the errors work differently on the atmospheric muon flux and neutrino flux. Therefore, it is important to estimate the error for the study of hadronic interaction, then for the calculation of the atmospheric neutrino flux. Note, we treat the interaction cross section separately from the dynamics of hadronic interaction.

As the atmospheric density profile, the US-standard '76 atm model [39] is generally used in the calculation of atmospheric neutrino flux, including the HKKM04 calculation. The density profile of the US-standard '76 atm model is compared with that of newer atmosphere model MSISE90 [41] as a ratio in Fig. 8. The MSISE90 is considered the more realistic atmosphere model, since it gives the position and time dependent atmospheric variations. In the left panel, we show comparison of the atmospheric density profile at Kamioka for different seasons. We find the maximum difference below 40 km is $\sim 10\%$ in summer
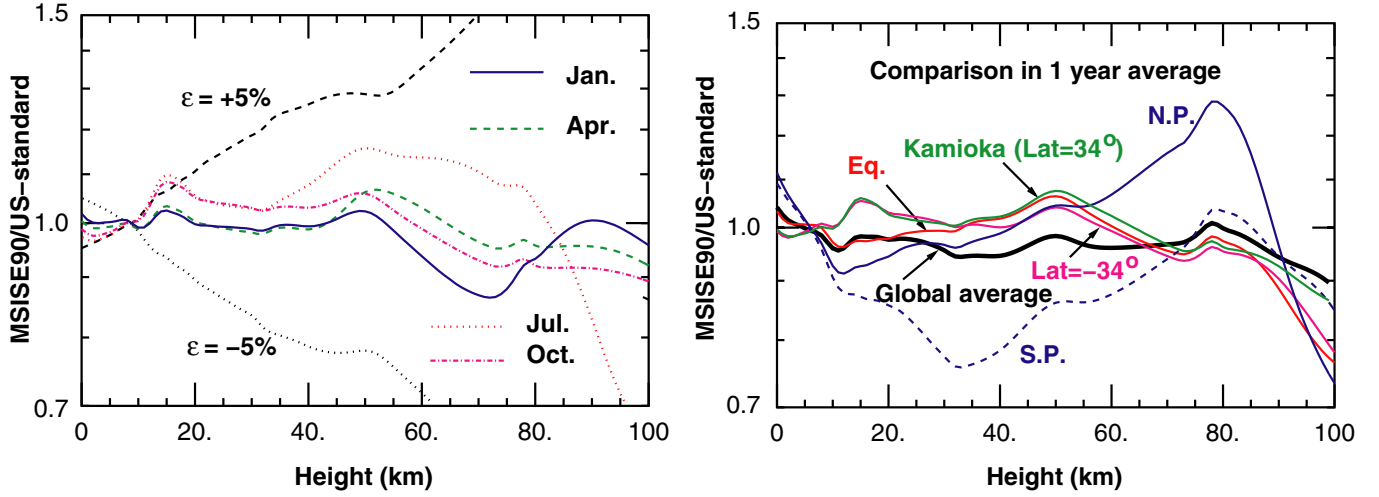
FIG. 8 (color online).   Left panel: the comparison of air density profile of MSISE90 [41] and US-standard '76 [39] in ratio at Kamioka in different seasons. The variations corresponding to $\varepsilon = \pm 5\%$ in Eq. (21) are also shown. Right panel: the same as the left panel, but at different latitude in all season average. The global average in the MSISE90 model is shown by the thick line.

(Jul.) and autumn (Oct.), but that the MSISE90 air density profile is very close to that of US-standard '76 in winter (Jan.) and spring (Apr.). In the right panel, we show the comparison of one-year-average at different latitudes (Lat $= -90$, -34, 0, 34, and 90), and the global average with the US-standard '76. The global average agrees well with the US-standard '76 within $\sim 5\%$ except for very high latitude.

To study the effect of the uncertainty of the air density profile, we consider the modification of the US-standard '76 air density profile as

$$\rho_{\mathrm{us},\varepsilon}(h) = \frac{1}{1+\varepsilon} \cdot \rho_{\mathrm{us}}\!\left(\frac{h}{1+\varepsilon}\right), \tag{21}$$

where $\rho_{\mathrm{us}}(h)$ is the atmospheric density profile of the US-standard '76, and h is the altitude. Note the static solution for compressible gas in the gravitational field is expressed as

$$\rho(h) = \rho_0 \cdot e^{-(h/h_s)}, \tag{22}$$

and the scale height h_s is proportional to the absolute temperature. Therefore, the ε in Eq. (21) corresponds to the change of the atmospheric temperature. We consider the variation of $\varepsilon = \pm 5\%$ in Eq. (21) for the seasonal variation. Actually, the variation from winter–spring to summer-autumn is approximately the same as the variation of $\varepsilon = 0 \sim +5\%$ below 20 km (Fig. 8). In Fig. 9, we plot the variation of atmospheric muon and neutrino fluxes as a ratio for the variation of $\varepsilon = \pm 5\%$ in Eq. (21).

Note, the variation of air density at the production height of π's and K's is the main reason for the variation of the fluxes of atmospheric neutrinos and high energy muons. The decay and the interaction are competitive processes for mesons (π's and K's), and they balance when [Flight Length Before Decay] $=$

[Interaction Mean Free Path], or

$$c\tau \cdot E/Mc^2 = A_{\mathrm{air}}/\sigma_m \rho N_a \tag{23}$$

is satisfied. Here, τ is the lifetime of the particle, E is the energy and M is the mass of the particle, A_{air} the average mass number of air nuclei, σ_m the interaction cross section of the meson and air nuclei, ρ the mass density of the air, and N_a the Avogadro constant. The production height is approximated by the first interaction height of cosmic rays, i.e. $A_{\mathrm{air}}/\sigma_{cr} N_a \sim 100$ g/cm^2 in the air depth, where σ_{cr} is the interaction cross section of cosmic rays. In the US-standard '76 atm model, it is calculated as ~ 16 km a.s.l. and the air density is $\sim 0.16 \times 10^{-3}$ g/cm^3, for vertical directions. The energies with which the decay and interaction balance are approximately 90 GeV for $\pi^{\pm}$, 170 GeV
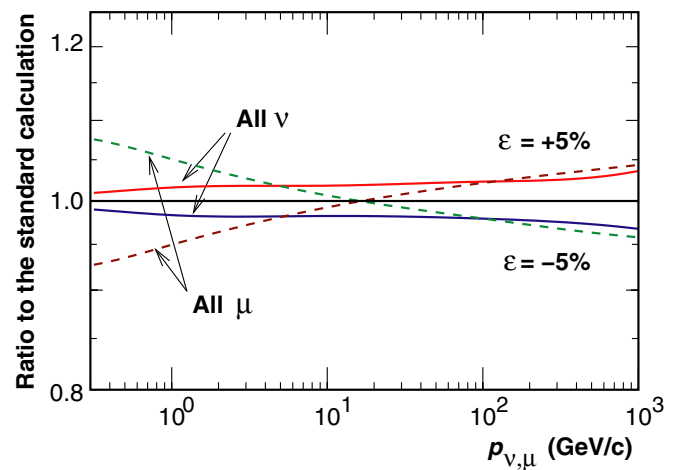

FIG. 9 (color online).   The variation of atmospheric muon and neutrino fluxes for a change of atmospheric density profile corresponding to the $\varepsilon \pm 5\%$ in Eq. (21) from the US-standard '76 atm model.

for K_L^0, and 690 GeV for $K^\pm$ there. Below these energies, most π's or K's decay producing the muons and neutrinos, and above these energies, most of them interact with the air nuclei, producing lower energy π's or K's. From Eq. (21), we find the air density at constant air depth decreases for $\varepsilon > 0$ and increases for $\varepsilon < 0$.

The actual production height of π's and K's is spread widely in the air depth, and so the air density there has a wide distribution. The variation of the atmospheric density profile changes the distribution a little, and works mildly on both neutrino and muon productions at higher momenta. With the variation of $\varepsilon = \pm 5\%$, the neutrino flux varies $\pm 1.5\%$ at 1 GeV, $\pm 1.8\%$ at 10 GeV, and $\pm 2.2\%$ at 100 GeV/c. From this variation, we estimate that the error due to the uncertainty of atmospheric density profile would be similar to these values or smaller.

The variation of muon flux at lower momenta could be explained by the change of production height with the muon decay. The production height approximated by the constant depth (~ 100 g/cm^2) moves to higher altitude for $\varepsilon > 0$ and lower for $\varepsilon < 0$, and so the muon flux increases for $\varepsilon < 0$, and decreases for $\varepsilon > 0$ at lower momenta. The variation with $\varepsilon = \pm 5\%$, is $\sim \mp 5\%$ at 1 GeV/c and larger at much lower momenta.

Note, there are short-term variations of atmospheric density profile due to the change of climate corresponding to $\varepsilon = \pm 5\%$ or more. They are crucial in the precise comparison of the calculation and observation of the atmospheric muon flux. In the following studies, we calculate the muon fluxes using the observed atmospheric density profile for the observation duration, when available.

At the higher momenta ($\gtrsim 100$ GeV/c), the variation of muon flux by the change of atmospheric density profile is smaller than the observation error of muon flux, even in the precision measurements. We use the US-standard '76 atm model in the calculation for these momenta.

A change in the cross section also changes the first interaction height, therefore, we expect a similar variation of lepton fluxes to the change in atmospheric density profile. However, the variation is a little different from that in the change of atmospheric density profile. In the static atmosphere model [Eq. (22)], the mean free path of mesons at the first interaction depth is calculated as

$$\lambda_m = \frac{A_{\text{air}}}{\sigma_m \cdot \rho \cdot N_a} = \frac{\sigma_{\text{cr}}}{\sigma_m} \cdot h_s \qquad (24)$$

in real length, where σ_m is m-meson interaction cross section. The production depth of leptons are well approximated by the mean free path of cosmic ray in the column density calculated as $\Lambda_{\text{cr}} = A_{\text{air}}/\sigma_{\text{cr}} N_a$. If we assume $\sigma_{cr}/\sigma_m \sim$ const, the change of interaction cross section does not affect the competition of decays and interactions [Eq. (23)]. We expect very small variation of atmospheric
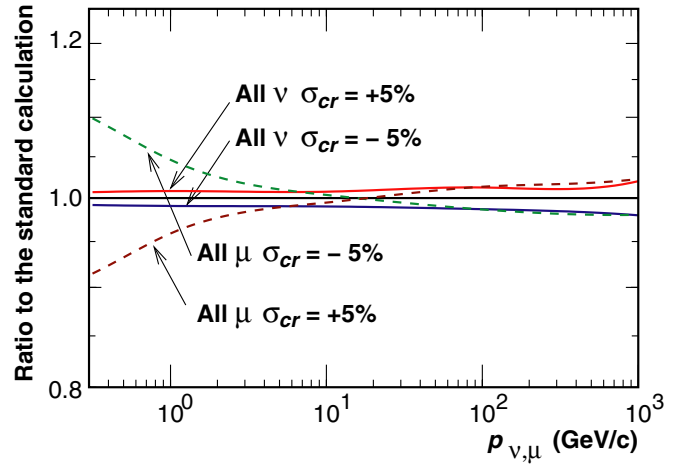

FIG. 10 (color online). The variation of atmospheric muon and neutrino fluxes resulting from a change of hadronic interaction cross section of $\sigma \pm 5\%$.

neutrino flux with $\sigma_{\text{cr}}/\sigma_m \sim$ const in the calculation with US-standard '76 or with MSISE90.

We study the effect of the uncertainties of the interaction cross sections ratio between cosmic rays and mesons, on the atmospheric muons and neutrinos. In Fig. 10 we show the ratios of the fluxes calculated with the variation of $\Delta\sigma_{\text{cr}} = \pm 5\%$ to the flux calculated with the standard cross sections, keeping the σ_m unchanged. The interaction cross section of nucleons are varied with that of cosmic rays. As expected, the variation of lepton flux is qualitatively the same with the variation due to the change of atmospheric density profile shown in Fig. 9, but quantitatively, the variation is smaller than that above 1 GeV/c. The variation of the atmospheric neutrino flux by the change of σ_{cr} of $\pm 5\%$ is about $\pm 2\%$ at higher momenta, and is smaller at lower momenta. The variation of the atmospheric muon flux at the change of σ_{cr} is the same at higher momenta, but is larger at lower momenta and in the opposite direction from that at higher momenta.

V. COMPARISON OF CALCULATED AND OBSERVED MUON FLUXES

In the left panel of Fig. 11, we plot the muon fluxes measured accurately at Tsukuba (Sept. 2002) [9] and on Mt. Norikura (Oct. 1999) [17] by the BESS group, and at CERN by the L3-Collaboration (L3 + C) [19] with the calculated muon fluxes in the HKKM04 scheme for Tsukuba and Mt. Norikura. (Details of these experiments are given in Sec. II.) In the right panel of Fig. 11, we plot the ratio [observation]/[calculation] for those precision measurements to compare the calculation and observation in more detail. In the calculation of the muon fluxes at Tsukuba and Mt. Norikura, we used the proton and helium fluxes measured by the BESS group in the preceding flight carried out within 2 months to take into account the solar modulation of cosmic rays correctly. Also, we used the
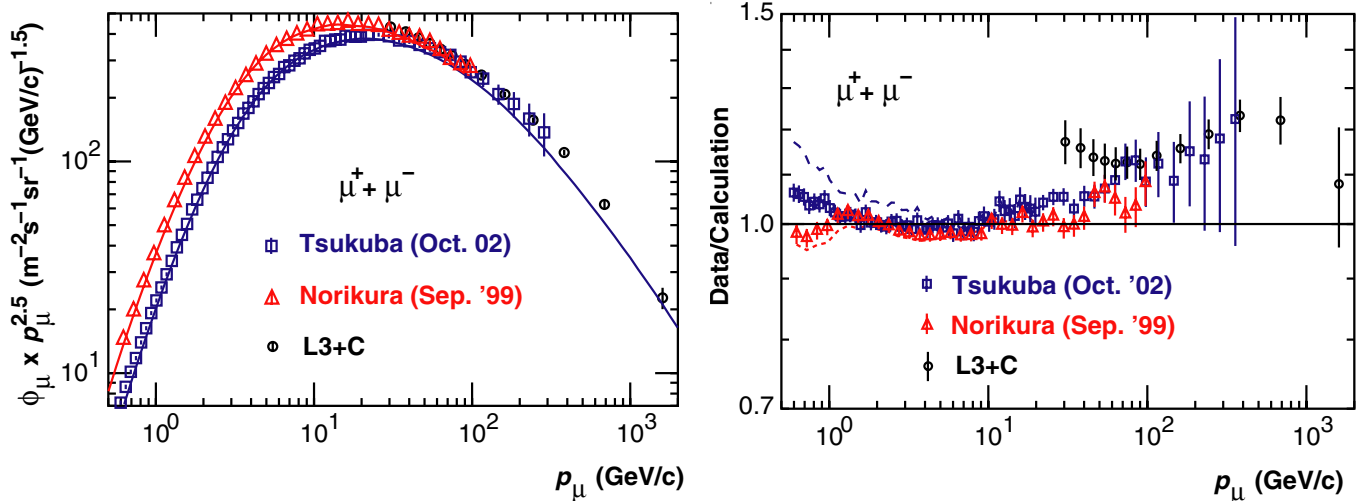
FIG. 11 (color online). Left panel: the muon fluxes measured accurately at Tsukuba (Sept. 2002) [9] and on Mt. Norikura (Oct. 1999) [17] by the BESS group, and at CERN by the L3-collaboration (L3 + C) [19] with the calculated HKKM04 muon fluxes for Tsukuba and Mt. Norikura. Right panel: the ratio of the muon flux data to the calculations. The dashed and dotted lines in the right panel are the same ratios but calculated with the US-standard '76 atmospheric model for Tsukuba and Mt. Norikura, respectively.

atmospheric density profile observed by the Japan Meteorological Agency [38] during the experimental periods for them. The calculations agree with the observations well ($\lesssim 5\%$) in the range $1 \sim 30$ GeV/c. Note, the calculation with the US-standard '76 atmospheric model is also compared with the observed muon data in the figure.

Below 1 GeV/c, there is a discrepancy between the two [observation]/[calculation] ratios calculated for Tsukuba and Mt. Norikura. This discrepancy might be explained by a different configuration of the BESS detector used for those two observations. As explained in Sec. II, an electron/positron component can be distinguished from muons in the Norikura observation with the electromagnetic shower counter, but not in the Tsukuba observation. Our Monte Carlo study for the observation predicts the electron and positron production at the roof of the experimental hall for Tsukuba experiment, and it explain at the difference of calculation and observation at least qualitatively.

In the muon observation at Norikura, surviving protons may affect the resultant muon flux. The [observation]/[calculation] ratio for Norikura shows some structure between 1 and 3 GeV/c, and is systematically smaller than that for Tsukuba above 3 GeV/c. This might be explained by the treatment of proton contamination in the positive muon candidates [17]. At sea level, the proton flux is much smaller than at mountain altitude, due to the attenuation in the atmosphere between the two altitudes. Therefore the correction is not necessary for Tsukuba experiment.

Thus, the muon fluxes in $1 \sim 30$ GeV/c are well understood by the HKKM04 calculation with the observed atmospheric density profile. We may conclude that DPMJET-III can be used to calculate the atmospheric neutrino flux in $1 \sim 10$ GeV region from the conclusion

in Sec. III. However, the muon flux calculated in the HKKM04 scheme is clearly smaller than those observed by the precision measurements above 30 GeV/c. At those momenta, it is difficult to understand the difference with the uncertainty of the physical inputs, such as the atmospheric density profile, other than the primary cosmic-ray model or the hadronic interaction model above 100 GeV. We note similar deficit is observed in the comparison of calculation with DPMJET-III and the observation of atmospheric gamma ray flux [42].

In Fig. 12, we show the comparison of the calculated muon charge ratio with the observed ones. We find the
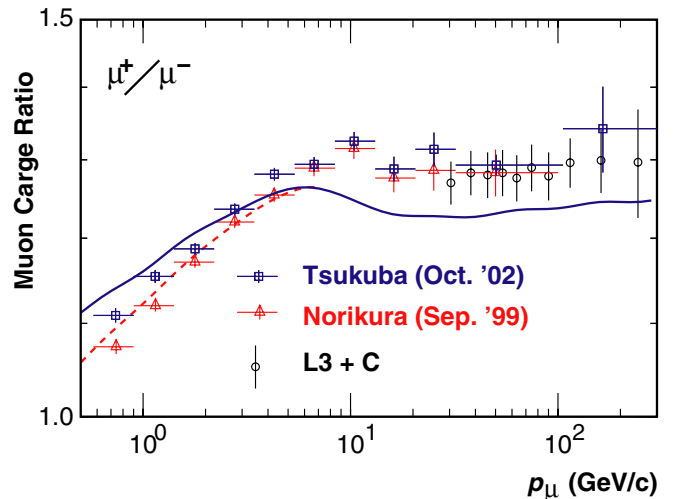

FIG. 12 (color online). Comparison of calculation and observation for muon charge ratio. Upper data and the solid line show the muon charge ratio at ground level (Tsukuba and L3 + C). Lower data and the dashed line show the same quantities for Mt. Norikura (2770 m a.s.l.).

agreement of the calculation and observation are better than 10% in the all energy region. However, the muon charge ratio is much more robust observation quantity, and reflects almost directly the π^+/π^- ratio of the hadronic interaction model. The difference indicates an error in the charge ratio of the π production in DPMJET-III.

The difference of muon charge ratio at different observation levels comes from the muon energy loss in the atmosphere. Most of muons are produced at higher altitudes than Norikura, and they are observed as slightly higher momenta muons at Norikura altitudes than at sea level, due to the muon energy loss.

VI. MODIFICATION OF DPMJET-III

Here we consider the modification of DPMJET-III [29], without discussing the dynamics of the hadronic interaction, and actually apply the modification to the "inclusive DPMJET-III" [24]. The inclusive DPMJET-III is constructed from the output of the original DPMJET-III, so that it reproduces the secondary spectra of the original DPMJET-III in an inclusive way. In this interaction model, the conservation laws are violated in each interaction, but are satisfied in the statistical way. Therefore, it is not useful to reproduce an event caused by a single cosmic ray, but is much faster than the original interaction model. The computation speed is very important in the calculation of the atmospheric neutrino flux.

Note, the region of $x \gtrsim 0.1$ in the π and K production is the most responsible for the atmospheric muons and neutrino fluxes (see Sec. III). We modify the gradient of the secondary spectra to cause changes at $x \sim 0.1$ for π's and K's without touching the multiplicities. Therefore, the quantum numbers are conserved automatically. For the magnitude of modification, we use the ratio of the average energy before and after the modification.

We assign a modification parameter to a valence quark of the projectile, and consider the same magnitude of modification for the secondary particles which have the same valence quark as the projectile. In p + Air interactions, the change of average energy are assigned as

$$\langle E_{\pi^+}\rangle = (1 + c_u)\langle E^0_{\pi^+}\rangle \qquad (u\bar{d})$$

$$\langle E_{\pi^-}\rangle = (1 + c_d)\langle E^0_{\pi^-}\rangle \qquad (d\bar{u})$$

$$\langle E_{\pi^0}\rangle = (1 + (c_u + c_d)/2)\langle E^0_{\pi^0}\rangle \qquad ((u\bar{u} - d\bar{d})/2)$$

$$\langle E_{K^+}\rangle = (1 + c_u)\langle E^0_{K^+}\rangle \qquad (u\bar{s})$$

$$\langle E_{K^-}\rangle = \langle E^0_{K^-}\rangle \qquad (s\bar{d})$$

$$\langle E_{K^0}\rangle = (1 + c_d)\langle E^0_{K^0}\rangle \qquad (d\bar{s})$$

$$\langle E_{\bar{K}^0}\rangle = \langle E^0_{\bar{K}^0}\rangle \qquad (s\bar{d}) \qquad (25)$$

Here, c_u and c_d are the modification parameters assigned to the u and d quarks, respectively, and the $\langle E^0_i\rangle$ is the average energy in the original DPMJET-III for the i particle. As the K^0 and $\bar{K}^0$ oscillate quickly, their average energies are

effectively modified as $\langle E_{K^0, \bar{K}^0}\rangle = (1 + c_d/2)\langle E^0_{K^0}\rangle$. Note, the modification of the nucleon spectra is determined after the modification for mesons are determined, so that the total energy is conserved to be equal to that of the projectile. These assumptions and parameterization naturally relate the K and π productions through the parameters assigned for the u and d quarks.

For the n + Air interactions, we assume isosymmetry, or that the parameter for the d-quark in n + Air interactions is equal to the c_u in Eq. (26), and that for the u-quark is equal to the c_d. As p + Air and n + Air are the major interactions in the cosmic ray propagation process in air, c_u and c_d are the two major parameters (Fig. 3).

For the energy dependence of c_i's, we consider polyline functions with kinks at 1, 3.16, 10, 31.6, 100, ... GeV. However, there are only a small number of data points above 100 GeV/c, and the uncertainty of the primary flux data is large there. We simply assume

$$c_i = a_i \cdot \log_{10}(E_{\text{proj}}/10 \text{ GeV}) \qquad (26)$$

above 316 GeV for $i = u$ and d. Then, we tuned the c_u's and c_d's at the kink points and a_u, a_d to minimize the difference between calculations and observations. In this study, we used the muon flux data from L3 + C at CERN above 60 GeV/c, and BESS at Tsukuba for all the momentum region. Note, the BESS data did not suffer from the effects of overlying material.

With these procedures, we find the c_u's and c_d's connected by the polylines in Fig. 13 give the best result. The kinks seen at around 10 GeV are due to the connection to the NUCRIN interaction model in Figs. 13 and 14. Note, the differences of c_u's and c_d's result from the difference in the muon charge ratio in the observation and calculation (Fig. 12). We call thus modified interaction model as "modified DPMJET-III."
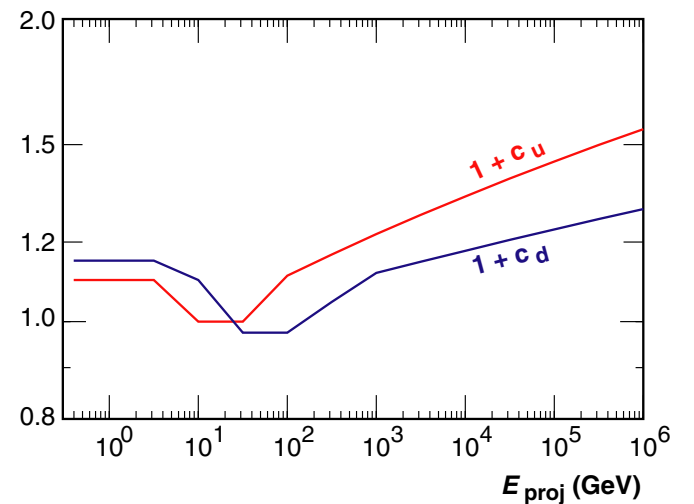

FIG. 13 (color online). The best modification parameters, c_u's and c_d's, as a function of E_{proj}.
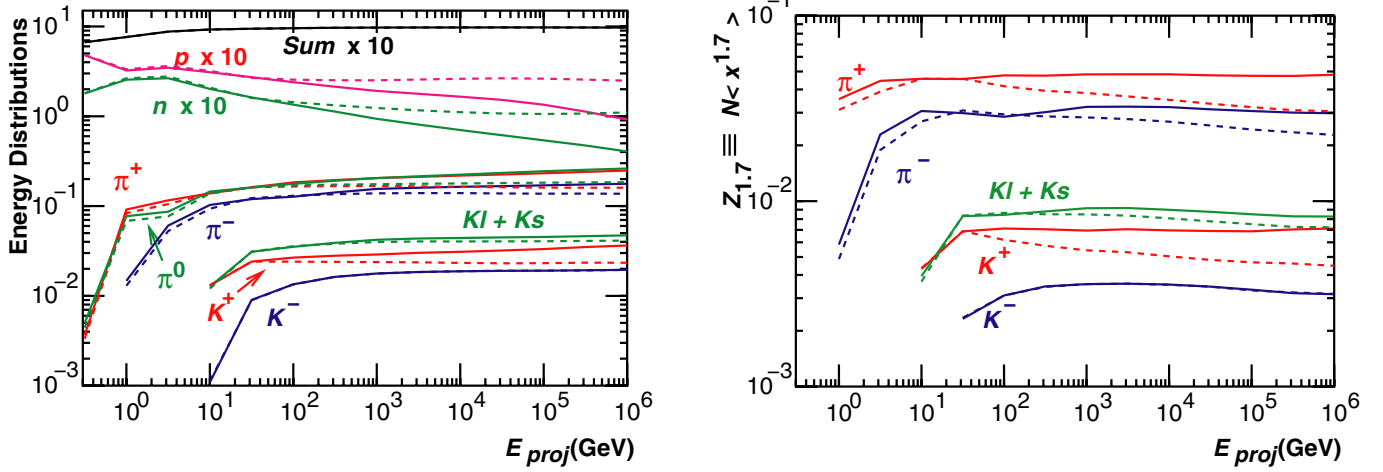
FIG. 14 (color online).   Left panel: The ratio of the average energy of secondary particles to the projectile energy. Right panel: the Z-factors for different kinds of particles. The Z-factor is defined in the text. In both panels, the solid lines show the modified ones, and dashed lines show the original ones.

We compared the energy distributions to the secondary particles of the original and modified DPMJET-III in the left panel of Fig. 14, and Z-factors in the right panel. The Z-factor is defined as

$$Z_i \equiv N_i \langle x_i^{1.7} \rangle \quad \text{and} \quad x_i \equiv \frac{p_i}{p_{\text{proj}}}, \qquad (27)$$

where N_i is the multiplicity and x_i is the scaling variable used in Sec. III for the i secondary particle (π^+, π^-, ...). The power 1.7 is approximately equal to the integral spectrum index of the cosmic-ray protons (1.71 in the primary flux model used by HKKM04). The Z-factor plays an essential role in the analytic calculation of the atmospheric muon and neutrino flux at higher energies. We find the Z-factors in modified DPMJET-III have flatter energy dependences than the original one above 100 GeV, as is suggested by the scaling hypothesis.

In Fig. 15, we compared the x_F spectra of π's production of p + Air interactions in the original and modified DPMJET-III with that of p + C interactions in the NA49 experiment at 158 GeV/c [30]. In this comparison, we use the Feynman scaling variable defined as $x_F = p_\parallel / 2\sqrt{s}$ in the CM-frame of a projectile and a nucleon in the target nucleus. Note, the scaling variable x we used in Sec. III is defined a little differently from the x_F using the momenta at the rest frame of Air nuclei. However, both definitions are almost equivalent for $x_F > 0.1$ at 158 GeV/c. We find the modified DPMJET-III reproduce the production spectra at $x_F \gtrsim 0.2$ better than the original DPMJET-III.
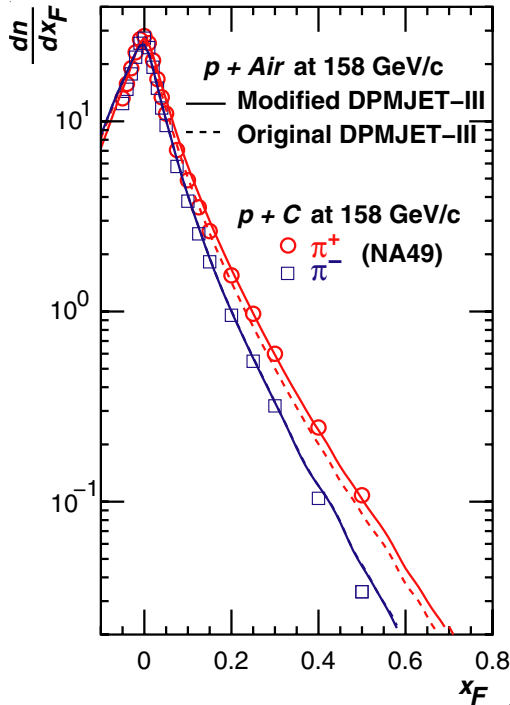

FIG. 15 (color online).   The comparison of the π's production spectra of the original and modified DPMJET-III in p + Air interaction with that in p + C from the NA49 experiment at 158 GeV/c. Note, the production spectrum of π^- of the modified DPMJET-III at 158 GeV/c is almost the same as that of the original DPMJET-III.

VII. THE CALCULATIONS WITH THE MODIFIED INTERACTION MODEL

In this section, we calculate the muon fluxes for the observations at Mt. Norikura, Tsukuba and CERN with the modified DPMJET-III described in the previous section. Except for the interaction model, we exactly repeat the calculations in Sec. V, i.e. we use the primary flux model based on the measurement within 2 months, and

observed atmospheric density profile during the experimental period for Mt. Norikura and Tsukuba. The muon flux sum ($\mu^+ + \mu^-$) is compared in ratio [observation]/[calculation] in the left panel of Fig. 16, and the muon charge ratio in the right panel. In the left panel, we also plotted the ratio for the horizontal muon flux data observed by the DEIS [31] and MUTRON [32] experiments.

Comparing Fig. 16 with Figs. 11 and 12, we find the agreement of calculation and observation of the muon fluxes is greatly improved by the modification in $30 \sim 300$ GeV/c for muon fluxes at Mt. Norikura and Tsukuba and between 60 GeV $\sim$ 2 TeV for the CERN experiment. We summarized the remaining differences between calculations with the modified DPMJET-III and observations, including the experimental errors, as

$$
\delta\Phi_\mu = \begin{cases} 0.04 - 0.24 \cdot \log\left(\frac{1\,\text{GeV}/c}{p_\mu}\right) & p_\mu < 1 \text{ GeV}/c, \\ 0.04 & 1 \text{ GeV}/c < p_\mu < 20 \text{ GeV}/c, \text{ and} \\ 0.04 + 0.065 \cdot \log\left(\frac{p_\mu}{20 \text{ GeV}/c}\right) & p_\mu > 20 \text{ GeV}/c, \end{cases} \tag{28}
$$

and plotted these in Fig. 16 with dashed lines. We also find DEIS and MUTRON data agree with the calculation in the momentum ranges of $60 \sim 600$ GeV/c and 200 GeV $\sim$ 2 TeV/c respectively, and are well inside the dashed lines. Note, the systematic error for DEIS and MUTRON are not included in the error bars. The modified DPMJET-III should be able to calculate the atmospheric neutrino flux, at least for the π-decay, with good accuracy above 1 GeV, from the study described in Sec. III.

VIII. SUMMARY

In this paper, we have studied the hadronic interaction for the calculation of atmospheric neutrino flux, using atmospheric muon flux data observed by precision measurements.

We summarized the muon data from the precision measurements, and selected the data from BESS and L3 + C for our study. There are other potentially useful data, such

as muon observations at balloon altitudes by BESS, or for horizontal directions by MUTRON or DEIS. However, the former still suffers from small statistics, and the latter do not clearly quantify the systematic errors in their reports.

Then, we studied the π and K productions in the hadronic interactions of cosmic rays and air nuclei relevant to the atmospheric muons and neutrinos. In this study we manipulated analytic expressions, but the actual calculations were carried out in the Monte Carlo simulation using the HKKM04 calculation code. With the Monte Carlo data being interpreted with the use of the analytic expressions, we found the atmospheric muon and neutrino fluxes originated from the π decay have the relation, $\Delta\Phi_\mu/\Phi_\mu \simeq \Delta\Phi_{\nu_\mu}/\Phi_{\nu_\mu} \simeq \Delta\Phi_{\nu_e}/\Phi_{\nu_e}$ for $\gtrsim 1$ GeV. This relation is useful to study the error in the hadronic interaction model using the atmospheric muon data.

As original DPMJET-III can reproduce the muon flux data in $1 \sim 30$ GeV/c with the HKKM04 calculation
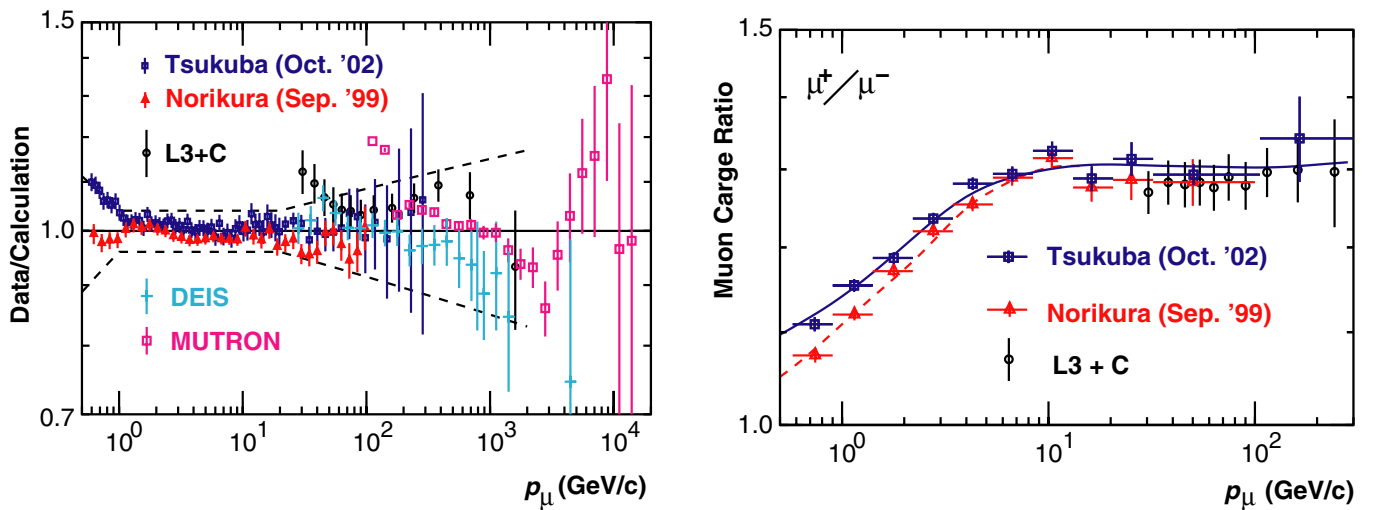

FIG. 16 (color online). The comparison of calculated muon fluxes with the modified interaction model and the observed ones. The dashed line is the sum of the errors in data and residuals by the modification [Eq. (28)]. Left panel: for the muon flux sum ($\mu^+ + \mu^-$), and right panel: for charge ratio (μ^+/μ^-). Note, the systematic errors for DEIS and MUTRON are not included in the error bars.

scheme, we may say that DPMJET-III is good interaction model to calculation the atmospheric neutrino flux in the $1 \sim 10$ GeV range. Note that π's are the main source both for atmospheric muons and neutrinos in this energy region. However, the observed muon data show a sizable deviation from the calculated muon flux above 30 GeV/c and in the muon charge ratio, suggesting room for improvement in the DPMJET-III model. We note similar deficit is observed in the comparison of calculation with DPMJET-III and the observation of atmospheric gamma ray flux [42].

We tried an improvement of the interaction model based on the quark parton model, and applied the modification to the "inclusive DPMJET-III." We have tuned the secondary spectra of the hadronic interactions, so that the calculation reproduces the observed muon fluxes accurately. As a result, the muon fluxes calculated with the modified interaction model agree very well with the observed muon flux data, up to ~ 1 TeV for both vertical and horizontal directions in the flux sum ($\mu^+ + \mu^-$) and up to 300 GeV/c in the charge ratio. The muon flux data for horizontal directions are potentially useful to examine the propagation code of cosmic rays in the atmosphere. However, the systematic error of the available muon flux data for hori-

zontal directions ware not studied well. We just show the comparison of calculation in the figure in this paper.

The calculation of atmospheric neutrino flux, and the robustness of our modification to the DPMJET-III model, will be described in the following paper [33]. Note, the K productions in the hadronic interactions are naturally modified through the modification for u and d-quarks. However, the modification of K productions weakly couple to the muon fluxes, and are not tested in the comparison of calculation and observation of muon flux below ~ 1 TeV. The uncertainty of K productions and the results in atmospheric neutrino flux calculation is also discussed in the following paper.

ACKNOWLEDGMENTS

[1] Y. Fukuda *et al.* (Super-Kamiokande Collaboration), Phys. Rev. Lett. **81**, 1562 (1998).

[2] Y. Ashie *et al.* (Super-Kamiokande Collaboration), Phys. Rev. D **71**, 112005 (2005).

[3] Y. Ashie *et al.* (Super-Kamiokande Collaboration), Phys. Rev. Lett. **93**, 101801 (2004).

[4] E. Aliu *et al.* (K2K Collaboration), Phys. Rev. Lett. **94**, 081802 (2005).

[5] J. Alcaraz *et al.* (AMS Collaboration), Phys. Lett. B **490**, 27 (2000).

[6] J. Alcaraz *et al.* (AMS Collaboration), Phys. Lett. B **494**, 193 (2000).

[7] T. Sanuki *et al.* (BESS Collaboration), Astrophys. J. **545**, 1135 (2000).

[8] M. Boezio *et al.*, Astropart. Phys. **19**, 583 (2003).

[9] S. Haino *et al.* (BESS Collaboration), Phys. Lett. B **594**, 35 (2004).

[10] T. K. Gaisser *et al.*, *Proceedings of the 27th International Cosmic Ray Conference, Hamburg* (2001), Vol. 5, p. 1643.

[11] P. K. F. Grieder, *Cosmic Rays at Earth* (Elsevier Science, New York, 2001).

[12] R. Bellotti *et al.*, Phys. Rev. D **53**, 35 (1996).

[13] R. Bellotti *et al.* (WiZard/MASS2), Phys. Rev. D **60**, 052002 (1999).

[14] M. Boezio *et al.* (WiZard/CAPRICE Collaboration), Phys. Rev. D **62**, 032007 (2000).

[15] M. Boezio *et al.*, Phys. Rev. D **67**, 072003 (2003).

[16] J. J. Beatty *et al.*, Phys. Rev. D **70**, 092005 (2004).

[17] T. Sanuki *et al.*, Phys. Lett. B **541**, 234 (2002), see also

erratum Ref. [43].

[18] K. Abe *et al.* (BESS Collaboration), Phys. Lett. B **564**, 8 (2003).

[19] P. Achard *et al.* (L3 Collaboration), Phys. Lett. B **598**, 15 (2004).

[20] G. T. Zatsepin and V. A. Kuzmin, Sov. Phys. JETP **14**, 1294 (1962).

[21] S. Hayakawa, *Cosmic Ray Physics* (John Wiley & Suns, New York, 1969), chap. 4.1.3,1, 4.1.3.2, pp. 402–406.

[22] A. Tam and E. Young, *Proceedings of the 11th International Cosmic Ray Conference, Budapest, 1969* (1969), Vol. 4, p. 306.

[23] D. H. Perkins, Astropart. Phys. **2**, 249 (1994).

[24] M. Honda, T. Kajita, K. Kasahara, and S. Midorikawa, Phys. Rev. D **70**, 043008 (2004).

[25] T. K. Gaisser and M. Honda, Annu. Rev. Nucl. Part. Sci. **52**, 153 (2002).

[26] K. Asakimori *et al.* (JACEE Collaboration), Astrophys. J. **502**, 278 (1998).

[27] V. A. Derbina *et al.* (RUNJOB Collaboration), Astrophys. J. **628**, L41 (2005).

[28] G. Fiorentini, V. A. Naumov, and F. L. Villante, Phys. Lett. B **510**, 173 (2001).

[29] S. Roesler, R. Engel, and J. Ranft, hep-ph/0012252.

[30] C. Alt *et al.* (NA49 Collaboration), hep-ex/0606028 [European Journal of Physics C (to be published)].

[31] O. C. Allkofer *et al.*, Nucl. Phys. **B259**, 1 (1985).

[32] S. Matsuno *et al.*, Phys. Rev. D **29**, 1 (1984).

[33] M. Honda *et al.*, following Article Phys. Rev. D **75**,

043006 (2007).

[34] K. Abe *et al.*, *Proceedings of the 28th International Cosmic Ray Conference, Tsukuba* (2003), Vol. 3, p. 1463, see also astro-ph/0312632.

[35] B. Nilsson-Almqvist and E. Stenlund, Comput. Phys. Commun. **43**, 387 (1987).

[36] H. Pi, Comput. Phys. Commun. **71**, 173 (1992).

[37] A. Fasso, A. Ferrari, P. R. Sala, and J. Ranft *Proceedings of the International Conference on Advanced Monte Carlo for Radiation Physics, Particle Transport Simulation and*

Applications (MC 2000), Lisbon, Portugal, 2000 (2001).

[38] Aerological data of japan, Japan Meteorological Agency.

[39] See http://nssdc.gsfc.nasa.gov/space/model/atmos/us_standard.html.

[40] There are many articles. For example, see http://en.wikipedia.org/wiki/B-spline.

[41] A. E. Hedin, J. Geophys. Res. **96**, 1159 (1991), also see http://nssdc.gsfc.nasa.gov/space/model/atmos/msise.html.

[42] K. Yoshida *et al.*, Phys. Rev. D **74**, 083511 (2006).

[43] T. Sanuki *et al.*, Phys. Lett. B **581**, 272 (2004).